FROM THE CURRENT LITERATURE

Electronic structure of silicon nitride

V A Gritsenko

Contents

Abstract. **Amorphous oxide SiO_2, oxynitride SiO_xN_y, and silicon nitride Si_3N_4 are the three key dielectric materials of silicon device technology. Silicon nitride is currently finding use in a variety of applications, in particular, as a storage medium in next-generation flash memory devices. Varying the chemical composition of nonstoichiometric silicon-rich SiN_x allows a wide-range control of its optical and electrical properties. In this review, an analysis of the electronic structure of silicon nitride of varying composition is presented.**

1. Introduction

The amorphous forms of silicon dioxide (SiO_2), silicon oxynitride (SiO_xN_y), and silicon nitride (Si_3N_4), the three key dielectrics used in silicon integral circuits, have enabled spectacular progress in semiconductor silicon electronics, which came to replace vacuum electronics. The first of these, silicon dioxide, with its low density of states at the silicon–dielectric interface ($\approx 10^{10}$ cm^{-2}), high atomic-scale breakdown field ($> 10^7$ V cm^{-1}), and low trap concentration, has an application as a subgate insulator in metal–dielectric–semiconductor (MDS) transistors.

Silicon nitride, in contrast, has very high concentrations of electron and hole traps ($\approx 10^{19}$ cm^{-3}) [1, 2], which are deep and have the energy $W \approx 1.5$ eV [3]. The memory effect exhibited by silicon nitride, i.e., the ability to trap electrons and holes injected into it, is characterized by the trapped

lifetime ≈ 10 yr at 85 °C and is used in the design of energy autonomous flash memory devices capable of retaining information even when switched off [4, 5]. The higher dielectric constant of nitride ($\varepsilon \approx 7$) compared to dioxide ($\varepsilon \approx 3.9$) makes the former useful as an insulating layer in the holding capacitors of read access memories, for insulating multilevel metal interconnections, or as a blocking dielectric in floating gate flash memory elements. Silicon devices use the amorphous form of silicon nitride.

Crystalline silicon nitride has applications as a ceramic owing to its high hardness, wear resistance (a requirement for cutting tools), strength, heat resistance, radiation resistance (needed in atomic energy and space applications), and low density (human bone prosthetics).

The mechanical, optical, and electrical properties of silicon nitride are determined by its electronic structure. The understanding of this structure has made considerable advances in recent years due to the progress in computer technology and owing to the development of complex *ab initio* quantum mechanical methods for simulating the electronic structure of solids. The aim of this review is to summarize the state of the art in the field.

2. Experimental approaches to the electronic structure of silicon nitride

Figure 1a is a schematic diagram of electronic transitions in Si_3N_4 obtained from spectroscopic data. Information on the partial density of states in the valence band is obtained from an X-ray emission spectroscopy experiment that measures the spectrum arising due to electrons dropping down to fill core shell (Si 1s, Si 2p, N 1s) vacancies (holes) (which form when an electron beam or an X-ray quantum is incident on the sample). The X-ray emission intensity is proportional to the electronic density of states in the valence band. The valence band of Si_3N_4 has a width of about 13.0 eV, which is much less than the X-ray transition energies observed in emission spectra. This suggests that the transition matrix element depends weakly on energy. The dipole approximation allows

V A Gritsenko Rzhanov Institute of Semiconductor Physics,
Russian Academy of Sciences,
pr. Lavrent'eva 13, 630090 Novosibirsk, Russian Federation
Tel. +7 (383) 333 38 64. Fax +7 (383) 333 27 71
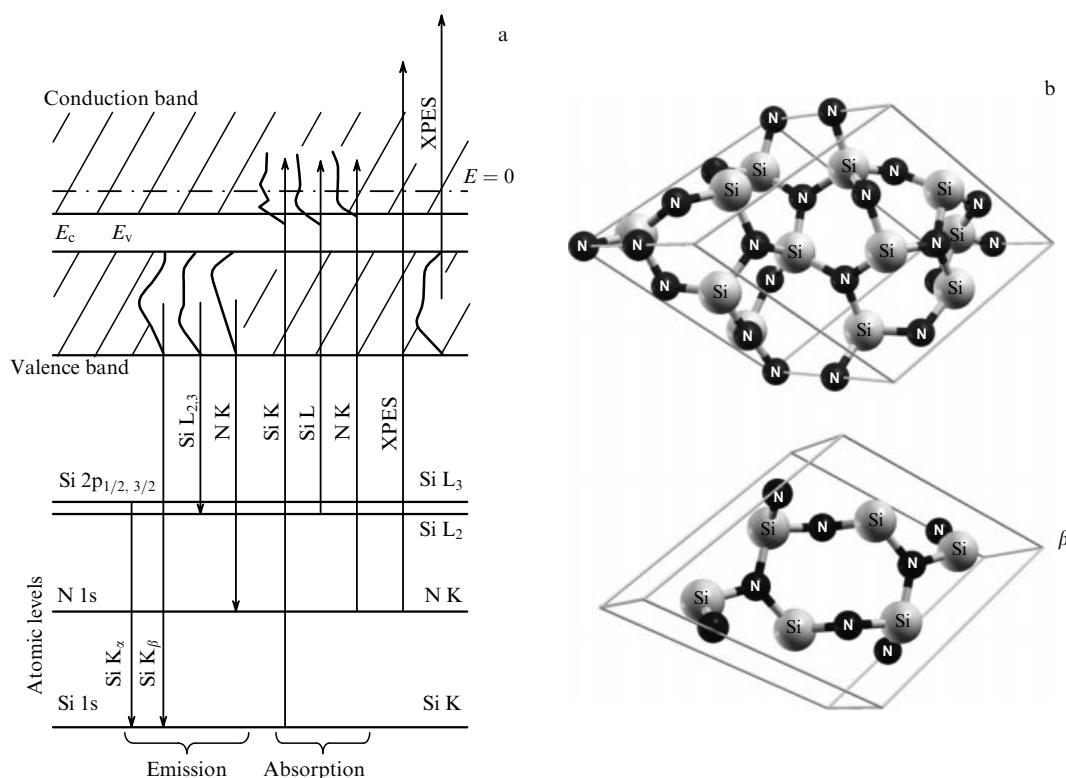E-mail: grits@isp.nsc.ru

Figure 1. (a) Schematic of electronic transitions observed in X-ray emission spectroscopy, X-ray photoelectron spectroscopy, and X-ray absorption spectra. Horizontal lines: atomic levels; vertical arrows: electronic transitions. (b) Unit cells of α-Si$_3$N$_4$ and β-Si$_3$N$_4$.

transitions with the orbital momentum changing by ± 1. The dipole selection rules for the emission spectra of Si limit the transitions to those from Si 3s and Si 3d valence band states to the Si 2p atomic level (spectroscopically classified as L$_{2,3}$). The Si K spectra show transitions from Si 3p valence band states to Si 1s atomic states. In the K emission spectra of nitrogen, transitions from the N 2p valence band states to the N 1s atomic state show up.

The density of states in the conduction band is investigated using X-ray absorption spectra or quantum yield spectra. In the latter, the registered transitions are those from filled Si 1s, Si 2p, and N 1s levels to the unfilled vacancy states of the conductance band. In the first approximation, quantum yield spectra can be interpreted in terms of the dipole selection rules.

X-ray and ultraviolet photoelectron spectra (respectively, XPES and UVPES) carry information on the core atomic levels and the filled states of the valence band. In XPES experiments, a fixed-energy (monochromatic) quantum incident on the sample causes the core and valence band electrons to be emitted into the vacuum, where their energy distribution is measured. Using the known energy of the quantum and the measured kinetic energy of the electrons, the position of the atomic core levels relative to the vacuum energy of the electrons can be determined, as can the density of states in the valence band. We note that valence band states originate from electronic states having wave functions with different symmetries. The cross section of the photoemission of an electron into the vacuum depends on the symmetry of the wave functions and on the excitation energy. Therefore, the photoelectron spectrum of the valence band is not equivalent to the valence band density of states calculated quantum chemically.

3. Structure of silicon nitride

Silicon nitride is a polymorphic compound that exists in four allotropic modifications. In the crystalline state, it exhibits two stable hexagonal phenakite phases, α-Si$_3$N$_4$ and β-Si$_3$N$_4$ (Fig. 1b), the former being stable above and the latter below 1150 °C. Both α-Si$_3$N$_4$ and β-Si$_3$N$_4$ have the atomic density $\rho = 3.1$ g cm^{-3}. The unit cell of the α phase contains 28 atoms (12Si and 16N), its lattice parameters are $a = 7.75$ Å and $c = 5.62$ Å, and its symmetry is $P31c$. The unit cell of the β phase contains 14 atoms (6Si and 8N), its lattice parameters are $a = 7.71$ Å and $c = 2.91$ Å [6], and its symmetry is $P6_3/m$. Both phases have a tetragonal structure with silicon four-coordinated by nitrogen and nitrogen three-coordinated by silicon. The tetrahedron has a distorted shape, with the Si–N bond length ranging between 1.70 and 1.74 Å, N–Si–N tetrahedral angle between 107.0° and 112.3°, and Si–N–Si dihedral angle between 117.0° and 122.5°. From the atomic structure standpoint, the α phase most closely approaches the amorphous nitride a-Si$_3$N$_4$ [1]. The density, about the same for both, is $\rho \approx 3.0$ g cm^{-3}. The structure of amorphous Si$_3$N$_4$ was analyzed in Ref. [6]. The recently discovered ultra-high density cubic modification c-Si$_3$N$_4$ [7–9] consists of SiN$_4$ tetrahedra and SiN$_6$ octahedra and has the density $\rho \approx 4.0$ g cm^{-3} [8].

4. Electronic structure of Si$_3$N$_4$: theory and experiment

First-principle calculations of the electronic band structure of the α and β phases of silicon nitride were performed in [10–13] using the density functional theory (DFT), currently the basic tool for such calculations. This theory (briefly outlined in

Ref. [14]) uses plane waves as a basis set and employs unit cell boundary conditions to account for the periodic structure of the crystal. The electronic configurations used in Si_3N_4 calculations are [Ne] $3s^2$ $3p^2$ $3d^0$ for Si and [He] $2s^2$ $2p^3$ for N. The indicated states are those of the valence shell, and [Ne] and [He] are core states. The core electrons are taken into account by using the ultrasoft Vanderbilt pseudopotentials. Calculations are performed using the Perdew–Burke–Ernzerhof (PBE) parameterization of the exchange correlation potential. The authors note that the band structures of the α and β phases are closely similar and that the electronic structure has its properties almost completely determined by short-range order. According to [10], the effective mass of holes in α-Si_3N_4 has the anomalously large value $m_h^* \approx 2.5 - 3.5 m_e$. Experimentally, both the electron and hole effective masses of amorphous nitride are in the range $m_e^* \approx m_h^* \approx (0.4 - 0.5) m_e$ [15–19].

The prediction in Ref. [10] for the charge transfer on the Si–N bond is $\Delta = 0.70e$, which is twice the experimental value $\Delta = 0.35e$ for amorphous Si_3N_4 [20]. In Ref. [11], while the hole effective mass of α-Si_3N_4 was found to be close to the experimental value $m_h^* \approx 0.55 m_0$, its electron counterpart was overestimated twofold. The charge transfer on the Si–N bond was $\Delta = 0.63e$, which is considerably above the experimental 0.35e. The effective masses in the α and β modifications were observed to differ considerably.

We note that no experimental study has been made of the effective masses and effective charges in the crystalline modifications of Si_3N_4. At the same time, it is known that the amorphous phase is structurally close to the crystalline α phase. Because the amorphous structure is difficult to model theoretically from first principles, most studies overwhelmingly use the crystalline α phase instead of the amorphous one. Calculations show that this approximation works very well.

Figure 2 shows the Brillouin zone for α-Si_3N_4. For the β phase, the picture is similar except that the reciprocal unit c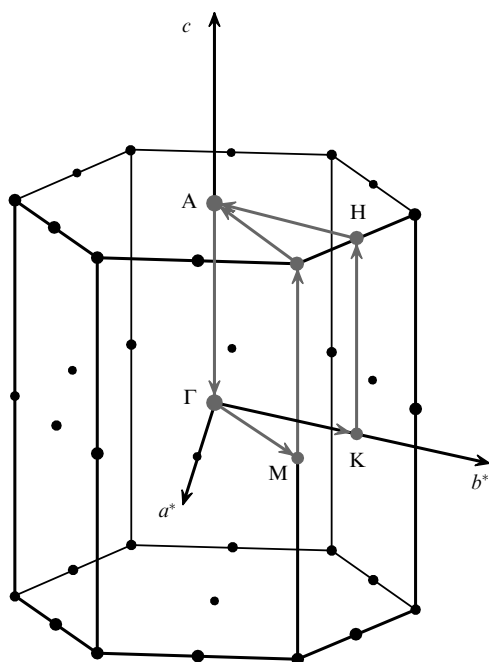ell is elongated along the hexagonal prism. The figure shows the unique symmetry points and the path in the reciprocal space along which the dispersion relation $E(k)$ shown in Fig. 3 (α-Si_3N_4) and Fig. 4 (β-Si_3N_4) was constructed.

The spatial electron density distributions were also calculated and analyzed for α-Si_3N_4 as a function of energy. Figure 5 reproduces the valence band charge density distribution for three different energies from Ref. [21]. Panel (a) shows the charge density distribution for energies in the neighborhood of the N 2s orbital level of -17 eV. In accordance with general quantum mechanical principles, the distribution pattern is nearly spherically symmetric, which is typical of the wave functions of s electrons. Panel (b) is the charge distribution for an energy of -4 eV, which corresponds to the N 2p–Si bonding orbital. It is seen that α-Si_3N_4 is a polar crystal, with the electron density on the S–N bond mainly localized near the highly electronegative nitrogen atom. The charge density gradient is along the Si–N bonds, implying the bonding nature of the orbital. Figure 5a depicts the electron density isosurface for nonbonding N $2p_\pi$ orbitals (of the energy -0.1 eV) that form the top of the valence band [12, 21]. As expected, the wave function of a nonbonding orbital is localized along the perpendicular axis to the plane formed by the nitrogen atom and its nearest environment of three silicon atoms.

The partial density of states (PDS) for Si 3s, 3p and N 2p in α-Si_3N_4 and β-Si_3N_4 was studied in [13]. The calculated PDSs of the two phases are quantitatively and qualitatively very similar. Based on Löwdin's population analysis, the
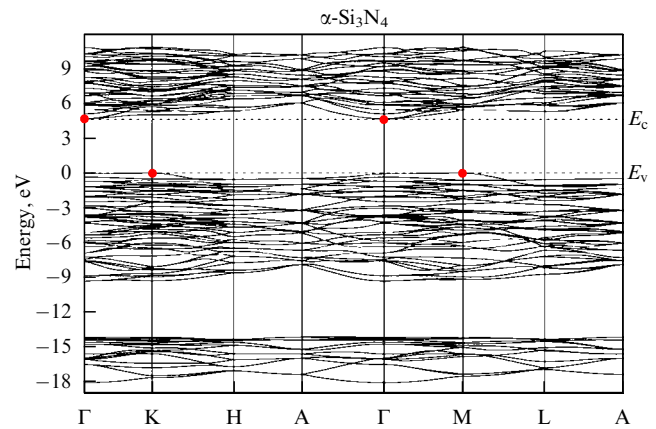

Figure 2. Brillouin zone of α-Si_3N_4, showing high symmetry points.

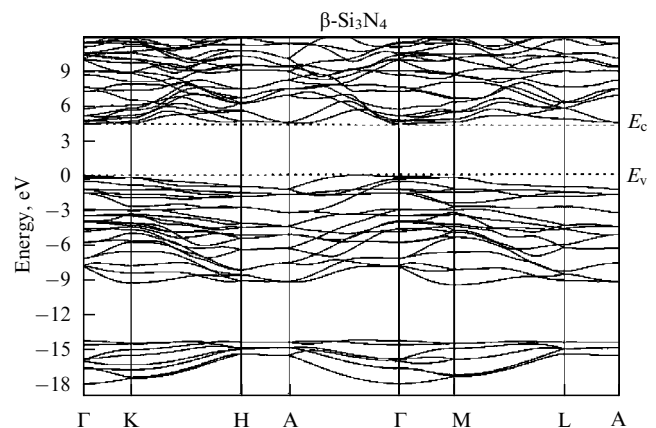**Figure 3.** Band structure of α-Si_3N_4.

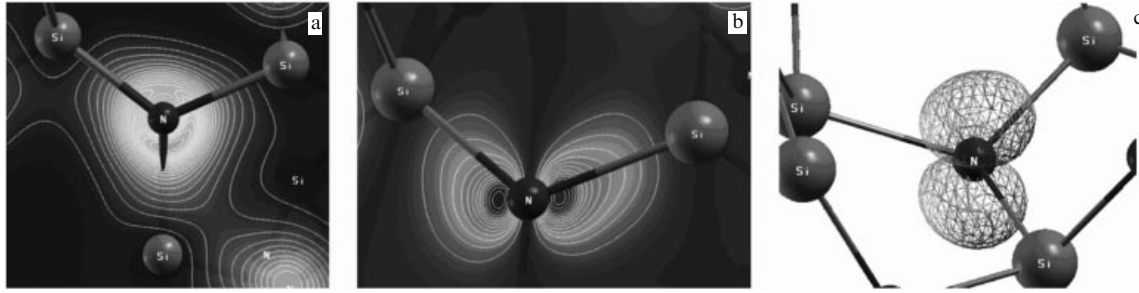**Figure 4.** Band structure of β-Si_3N_4.

Figure 5. Electron density distribution in α-Si$_3$N$_4$ for various energies: (a) 17 eV, (b) 4 eV, (c) 0.1 eV. Energy is measured from the top of the valence band.

Table. Electron and hole effective masses (in units of m_0) perpendicular ($m_{\mathrm{e}}^{*\perp}$, $m_{\mathrm{h}}^{*\perp}$) and parallel ($m_{\mathrm{e}}^{*\parallel}$, $m_{\mathrm{h}}^{*\parallel}$) to the hexagonal axis.

Effective mass tensor components	α-Si$_3$N$_4$		β-Si$_3$N$_4$	
$m_{\mathrm{e}}^{*\parallel}$	0.79 ($\Gamma - A$)		0.23 ($\Gamma - A$)	
$m_{\mathrm{e}}^{*\perp}$	1 ($\Gamma - K$; $\Gamma - M$)	0.5 ($\Gamma - K$; $\Gamma - M$)	1.6 ($\Gamma - K$; $\Gamma - M$)	
$m_{\mathrm{h}}^{*\parallel}$	0,5 (M $-$ L)		2.9 (top of B3 $-\Gamma$)	1.5 (top of B3 $-A$)
$m_{\mathrm{h}}^{*\perp}$	6 (M $-\Gamma$; M $-$ K)		0.85 (perpendicular to $\Gamma - A$)	

Note. For α-Si$_3$N$_4$, with degeneracy at the conduction band bottom (which is lifted along the hexagonal axis), the table gives two values of $m_{\mathrm{e}}^{*\perp}$ corresponding to the two degenerate bands. For β-Si$_3$N$_4$, where the m_{h}^{*} component (parallel to the axis of the prism) depends on the direction along the axis, two values of $m_{\mathrm{h}}^{*\parallel}$ are given.

effective charges on silicon and nitrogen atoms in α-Si$_3$N$_4$ are Si ($q = 2.49e$) and N ($q = 6.02e$). In Si$_3$N$_4$, silicon is four-coordinated by nitrogen and nitrogen is three-coordinated by silicon, and the calculated charge transfer onto an Si–N bond is therefore $\approx 0.37e$. This is close to the experimental value $0.35e$. The effective charges and the charge transfer onto the Si–N bond in β-Si$_3$N$_4$ differ little, or not at all, from their α-Si$_3$N$_4$ counterparts.

The values of electron and hole effective masses in both modifications of Si$_3$N$_4$ are listed in the table. Analysis of the band structure of α-Si$_3$N$_4$ suggests that this compound is an indirect band dielectric with the top of its valence band located at the K point of the Brillouin zone. The energy values are close to one another in all of the ΓKM plane (which is perpendicular to the axis of the prism; see Fig. 2). As a consequence, thee effective hol masses m_{h}^{*} have large values in this plane. The value of m_{h}^{*} in the direction perpendicular to the ΓKM plane is $\approx 0.5m_0$, which is close to the experimental value $(0.4-0.5)\,m_0$ [15].

The conduction band has its bottom at the center of the Brillouin zone, the Γ point (see Figs 3, 4). The degeneracy that occurs here is lifted as we move perpendicular to the axis of the prism (directions $\Gamma \rightarrow M$ and $\Gamma \rightarrow K$), but not when we move parallel (direction $\Gamma \rightarrow A$). Neglecting this degeneracy leads to a twofold overestimation of the electron effective mass [10], whereas taking it into account yields $m_{\mathrm{e}}^{*} \approx 0.5m_0$ for 'light' electrons, which is close to the experimental value $(0.4-0.5)\,m_0$. The band gap of α-Si$_3$N$_4$ is calculated to be 4.5 eV, in good agreement with both optical measurements on amorphous silicon nitride [2] and barrier measurements for electron and hole injection [15].

Similarly to α-Si$_3$N$_4$, β-Si$_3$N$_4$ is also an indirect dielectric, but considerable differences are revealed by the band structure analysis (see Fig. 4). Notably, the valence band has its top shifted from β-Si$_3$N$_4$ towards point A. Figure 6 shows a constant-energy surface in the Brillouin zone for β-Si$_3$N$_4$.
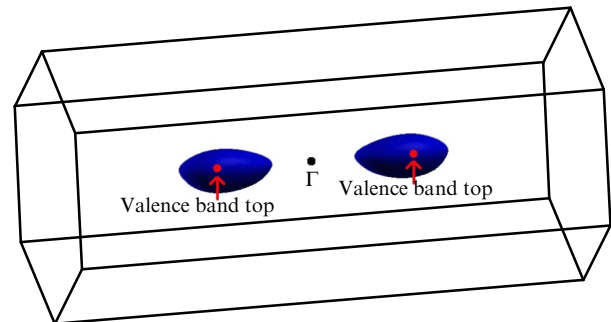

Figure 6. Constant energy surface in the β-Si$_3$N$_4$ Brillouin zone.

It is clearly seen that the constant-energy surface has the form of an ellipsoid of revolution, half of which is flattened along the axis of the hexagonal prism. The form of the dispersion $E(k)$ and the effective mass depend on the direction along the prism axis. Because the top of the β-Si$_3$N$_4$ valence band is not at a Brillouin symmetry point, the effective hole masses are dramatically different from those in α-Si$_3$N$_4$. The bottom of the conduction band of β-Si$_3$N$_4$ is at the Γ point of the Brillouin zone. In contrast to α-Si$_3$N$_4$, no degeneracy is observed.

Presented in Fig. 7 are the experimental results in Ref. [13] (reduced to a common energy scale, with the valence band top Si$_3$N$_4$ as energy zero) on the emission and absorption spectra of amorphous E_{v}. Based on the experiment, the valence band of Si$_3$N$_4$ consists of two subbands separated by an ion gap. The standard interpretation is that the lower valence band is formed by 2s orbitals of nitrogen mixed with 3s and 3p silicon states. The orbitals contributing to the upper valence band are nitrogen 2p and silicon 3s and 3p. The dipole-allowed transitions to the Si 2p level are those from the Si 3s states (single-center local transitions). The upper peak in the PDS
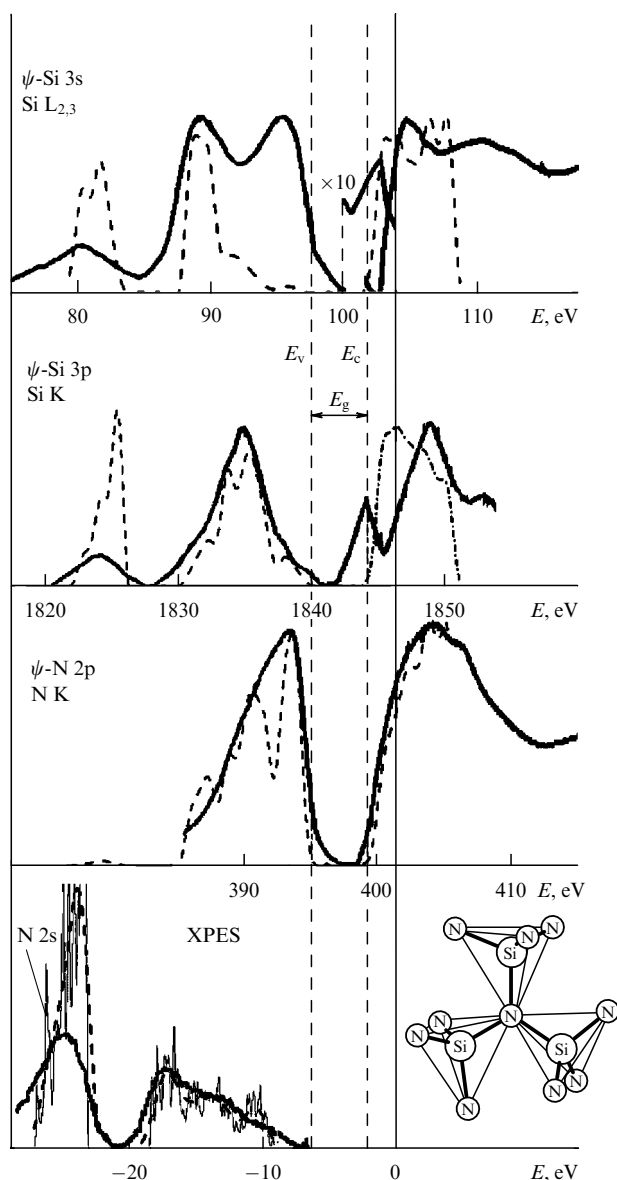
Figure 7. Experimental X-ray emission and quantum yield (absorption) spectra of amorphous Si_3N_4 (solid lines) and calculated partial density of states of α-Si_3N_4 (dashed lines). All spectra are reduced to a common energy zero, the electron energy in the vacuum. Bottom left: X-ray photoelectron spectrum of the valence band, the excitation energy $E = 1486.6$ eV. Bottom right: the elementary structural unit of silicon nitride, three tetrahedra linked by a nitrogen atom; ψ is the wave function.

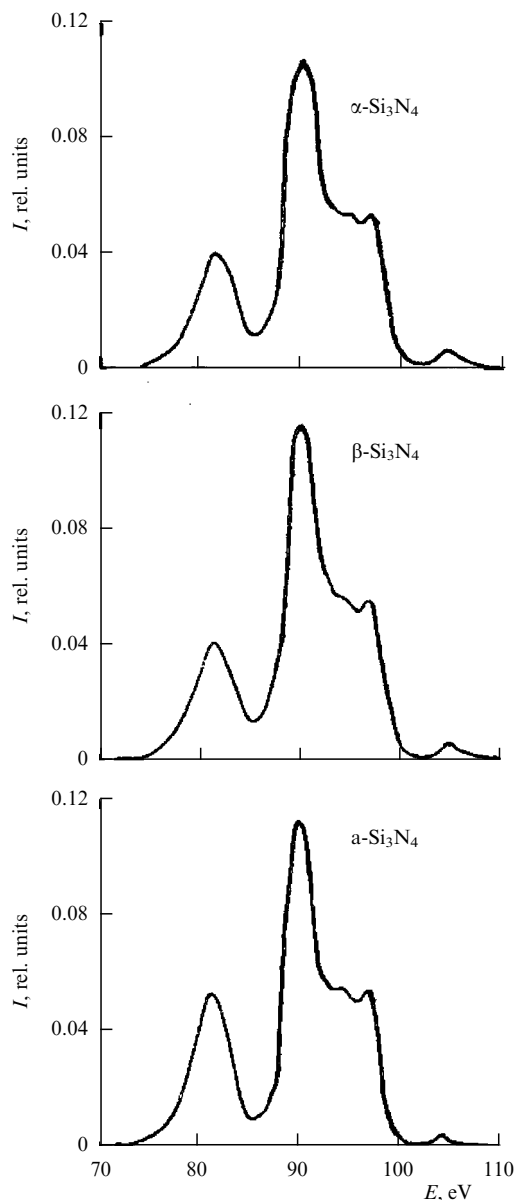**Figure 8.** Experimental Si $L_{2,3}$ emission spectra of various allotropic phases of silicon nitride.

orders, and amorphous α-Si_3N_4 has no long-range order at all. This points to the short-range order as a basic determinant of the electronic structure of silicon nitride.

5. Valence band structure from photoelectron spectroscopy

Figure 9 shows the photoelectron valence band spectra of amorphous Si_3N_4 measured for a number of synchrotron radiation excitation energies (40.8, 200.0, 384.0, 620.0, 1486.6 eV) [21]. Also shown in the figure are the valence band photoelectron spectra of α-Si_3N_4 calculated using the partial density of states obtained taking the excitation-energy-dependent photoionization cross section into account [24]. Calculations show that the valence band of silicon nitride consists of two subbands. The lower band is formed by N 2s orbitals mixed with Si 3s and Si 3p orbitals. We note that the spectral peak corresponding to the lower valence band was predicted to have a higher intensity than the experimental
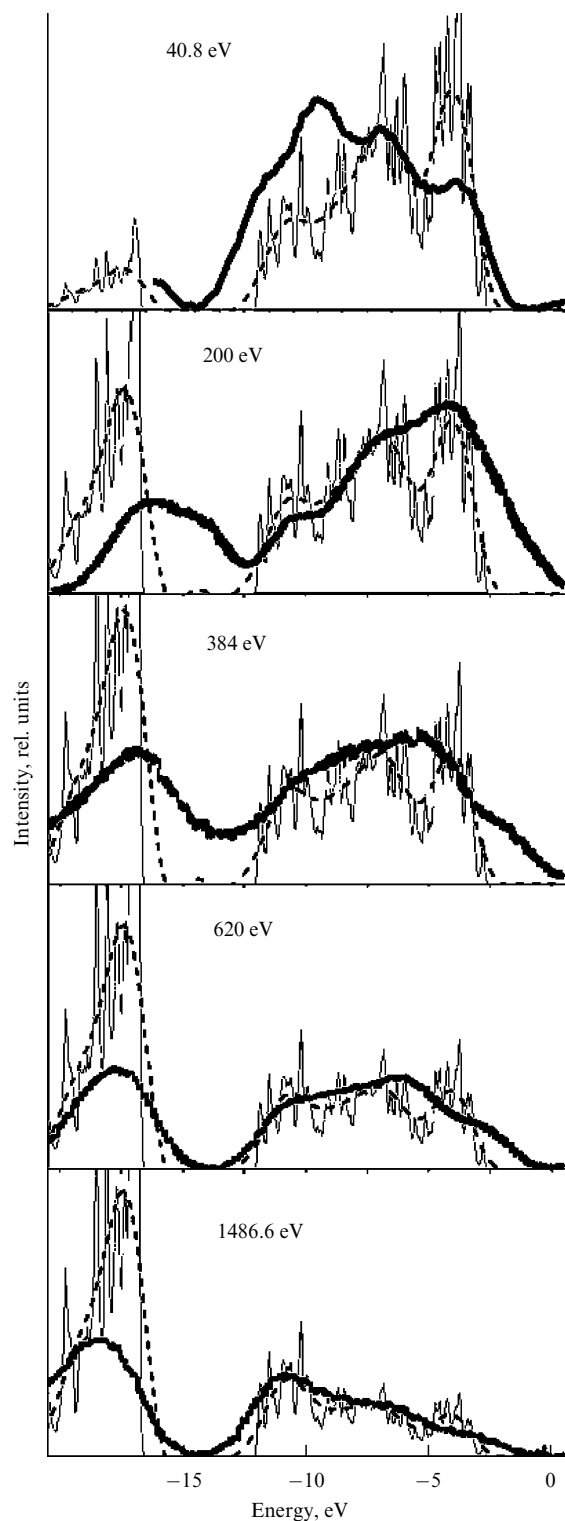
occurs at an energy of about -8 eV, a position close to that of its counterpart in the emission spectrum of Si $L_{2,3}$. The peak at about -3 eV in the experimental emission spectrum of Si $L_{2,3}$, as shown in Ref. [22], is due to contributions from the Si 3d states that are empty in a free silicon atom and from two-center transitions. The correct interpretation of the emission spectrum of Si $L_{2,3}$ requires an exact calculation of the dipole transition matrix elements with contributions from nonlocal (two-center N 2p 2p $\rightarrow$ Si) transitions included. A more accurate inclusion of these transitions is made in Ref. [22].

A comparison of the Si $L_{2,3}$ emission spectrum of crystalline α-Si_3N_4, β-Si_3N_4 with that of amorphous silicon nitride a-Si_3N_4 revealed their similarity (Fig. 8) [23]. These phases have a similar short-range-order arrangement of atoms, but α-Si_3N_4 and β-Si_3N_4 show different long-range

Figure 9. Experimental and calculated photoelectronic spectra of the valence band of amorphous Si_3N_4 for various excitation energies.

Figure 10. Interband transition spectrum and level ionization spectra in amorphous silicon nitride.

Similarly to the case of silicon dioxide, the top of the upper valence band of silicon nitride is dominantly formed by nonbonding N $2p_\pi$ orbitals. Because the overlap integral of the N $2p_\pi$ orbitals is small, heavy holes correspond to these orbitals near the top of the valence band, $m_h^* \approx 25 m_e^*$ (see the table). Such an interpretation was proposed in Ref. [25] for SiO_2. A fundamental point to note, however, is that together with N 3 orbitals, the Si 3s, Si 3p–N 2p bonding orbitals participate in forming the upper valence band. Corresponding to the Si orbitals near the top of the valence band are light holes ($m_h^* \approx 0.43 m_e^*$) (see the table).

6. Electronic transition energy diagram of amorphous Si_3N_4

Figure 10 shows the spectrum of excitations of electrons from the valence to the conduction band and from Si 2p and N 1s levels to the valence band in silicon nitride [26]. These data were used to build an electron transition energy diagram for silicon nitride. The reflection spectra of Si_3N_4 show only one feature at 9.5 eV (Fig. 11) [27], close to 9.3 eV observed in excitation spectra.

Figure 12 shows an energy diagram of the electronic states and X-ray transitions in amorphous Si_3N_4. The zero of energy is taken to be the electron vacuum level. The energies of the inner Si 2p, Si 2s, and N 1s levels were determined by X-ray photoelectric spectroscopy, and the energy of the Si 1s level was obtained from the Si K_α emission spectrum, in which transitions between the Si 2p and Si 1s levels are registered. The energy of this transition in Si_3N_4 is 1740.5 eV [1]. The horizontal lines in the valence and conduction bands in Fig. 12 are the energy positions of the density-of-states peaks

value, a consequence perhaps of an overestimation of calculated photoionization cross sections of the N 2s states.

The upper valence band is formed by N 2p and Si 3s and 3p orbitals. Both experiment and calculation reveal three peaks, of which the lower, the middle, and the one near the band top respectively correspond to Si 3s–N 2p bonding states, Si 3p–N 2p bonding states, and N $2p_\pi$ nonbonding states. The valence band energy distribution shown in Fig. 5 for a number of energies confirms this interpretation.
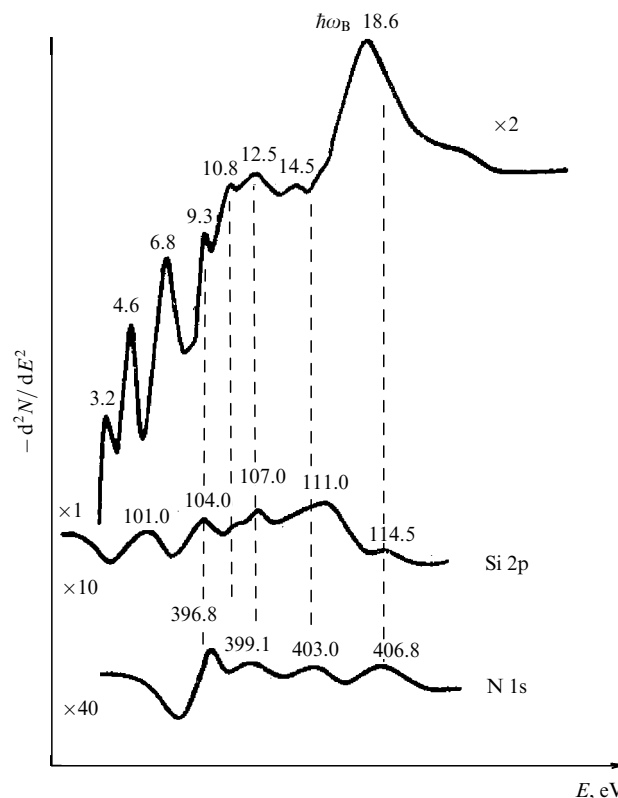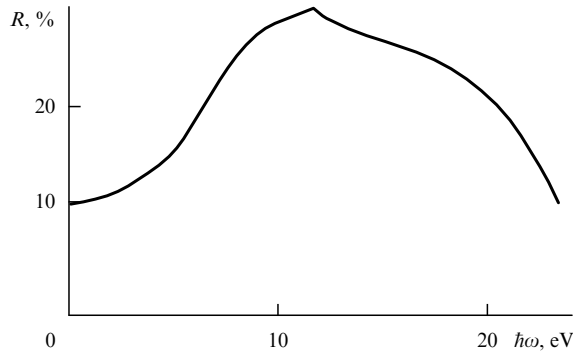
Figure 11. Reflection spectrum of amorphous Si₃N₄.

observed in X-ray transitions. Figure 12 shows electronic transitions observed in the X-ray emission and absorption spectra, as well as those observed in the ionization spectra of Si 2p and N 1s levels, and valence-to-conduction interband transitions (the latter taken from Ref. [26]). The low-energy edge of the Si $L_{2,3}$ quantum yield spectrum falls into the band gap. Also localized in the band gap is the low-energy (1844.4 eV) peak in the Si K quantum yield spectra. Added to this are the transitions observed in the ionization spectra at energies $E = 101.0$ and 104.0 eV (corresponding to the excitation of the Si 2p level) and at energies $E = 390.8$ and 399.1 eV (excitation of the N 1s level) (see Fig. 12). These peaks have no explanation in the one-electron framework, which does not consider defects and multielectron effects that stem from the present silicon nitride context. The nature of low-energy transitions in the quantum yield and ionization spectra awaits further research.

It follows from Fig. 12 that the transitions at $E = 9.3$, 10.8, and 14.5 eV coincide with the energy gap between the

bonding and nonbonding states. The transitions at 6.8 eV and 12.5 eV correlate poorly with the density-of-states peaks observed in X-ray transitions. We emphasize that the energy diagram in Fig. 12 is empirical, developed within an approach worked out for SiO_2 [28].

7. Electronic structure of silicon-enriched SiN_x

Amorphous silicon nitride is produced at high temperatures by pyrolysis (thermal decomposition) of silicon-containing (silane (SiH_4)) dichlorsilane (SiH_2Cl_2)) and nitrogen-containing (ammonia (NH_3)) gases, their partial pressure ratio determining the composition of the product. When there is a large excess of ammonia, silicon nitride has a composition close to that of stoichiometric Si_3N_4. As the relative pressure of silicon-containing gases increases, silicon nitride becomes enriched with silicon and its formula becomes SiN_x ($x < 4/3$). At its extremes, the structure of SiN_x is described either by the random bonding model or by the random mixture model [29, 30]. In the former, the structure of SiN_x is made up of tetrahedra of five compound species: SiN_vSi_{4-v}, $v = 0, 1, 2, 3, 4$, with silicon atoms randomly replacing nitrogen atoms in an SiN_vSi_{4-v} tetrahedron. In the latter model, it is made up of tetrahedra of two species, SiN_4 and $SiSi_4$, i.e., of two phases: Si_3N_4 and Si. Photoelectron spectroscopy experiments reveal that SiN_x is made up of tetrahedra of five species (SiN_vSi_{4-v}, $v = 0, 1, 2, 3, 4$); however, the statistics of the tetrahedra is not described quantitatively by the random bonding model. An intermediate model for the structure of SiN_x is proposed in Ref. [30].

Photoelectron spectroscopy was used in [31, 32] to investigate the electronic structure of the valence band of SiN_x. Figure 13 shows the X-ray photoemission spectra of the valence band of SiN_x of variable composition.
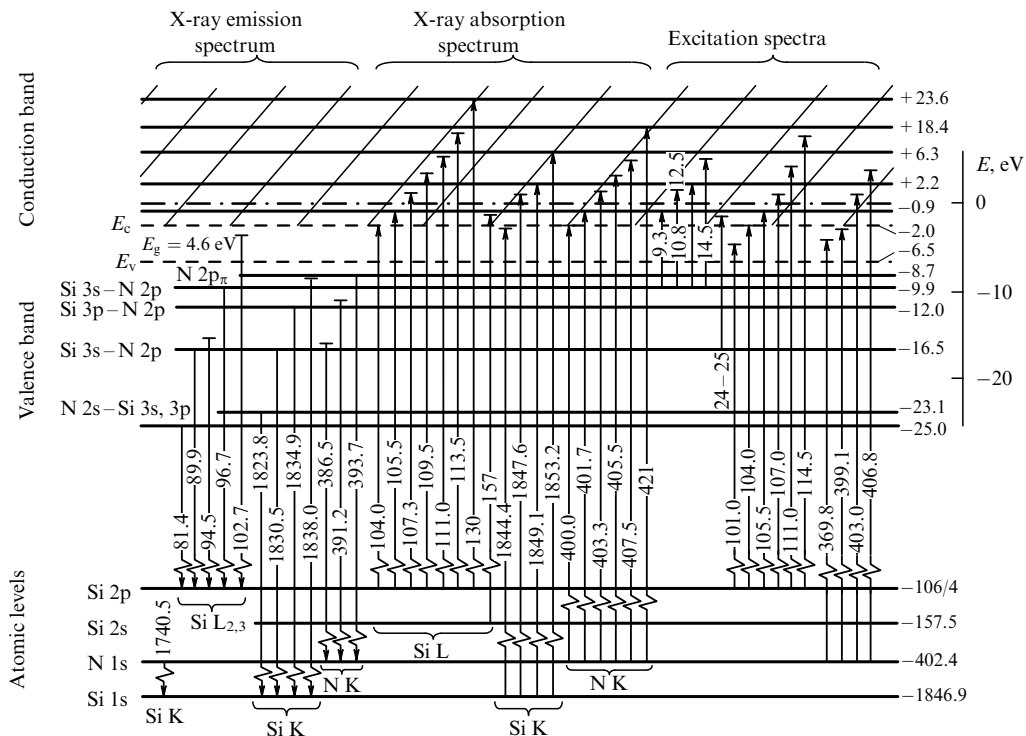

Figure 12. Electronic transitions in amorphous Si₃N₄ (schematic). Horizontal lines: positions of atomic levels and electronic density-of-states peaks in the valence and conduction bands; vertical arrows: electronic transitions.
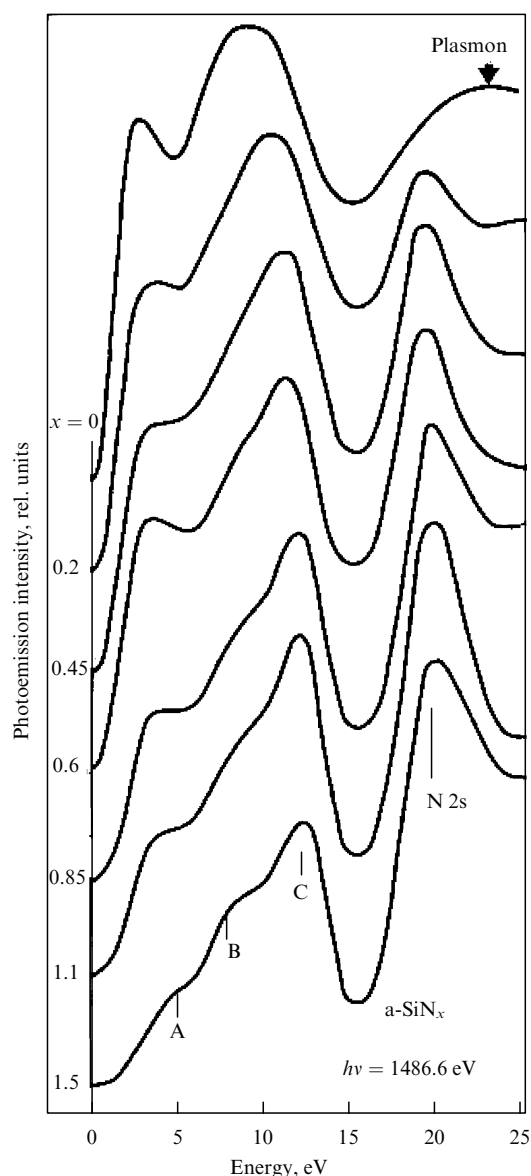
Figure 13. X-ray photoelectron spectra of the valence band of SiN_x.

Enriching with silicon shifts the top of the valence band E_v monotonically toward the band gap. The analysis of photoionization cross sections at 1486.6 eV indicates that at this quantum energy, silicon 3s and 3p states contribute most to photoionization. As can be seen in Fig. 14, ultraviolet photoionization spectra upon excitation by a 40.8 eV quantum exhibit a similar shift of the top of the valence band toward the band gap [32]. For a quantum of that energy, the dominant contribution to photoionization is due to nitrogen 2p states. Thus, enriching SiN_x with silicon shifts the bonding Si 3s, 3p–N 2p orbitals toward the band gap.

Interestingly, for a wide composition range of tetrahedral silicon compounds [Si, Si_3N_4, SiO_xN_y, SiO_2 [1], and SiN_x (Fig. 15)], the high-energy edge in Si $L_{2,3}$ emission spectra does not shift toward the band gap. While at first glance contradictory, this finding is explained by the fact that the Si 2p levels undergo a chemical shift toward high energies as atoms in the tetrahedral environment of a silicon atom become more electro-negative (Fig. 16).

As shown in Ref. [31], enriching SiN_x with silicon shifts the Si $L_{2,3}$ absorption edge toward lower energies (see Fig. 15),
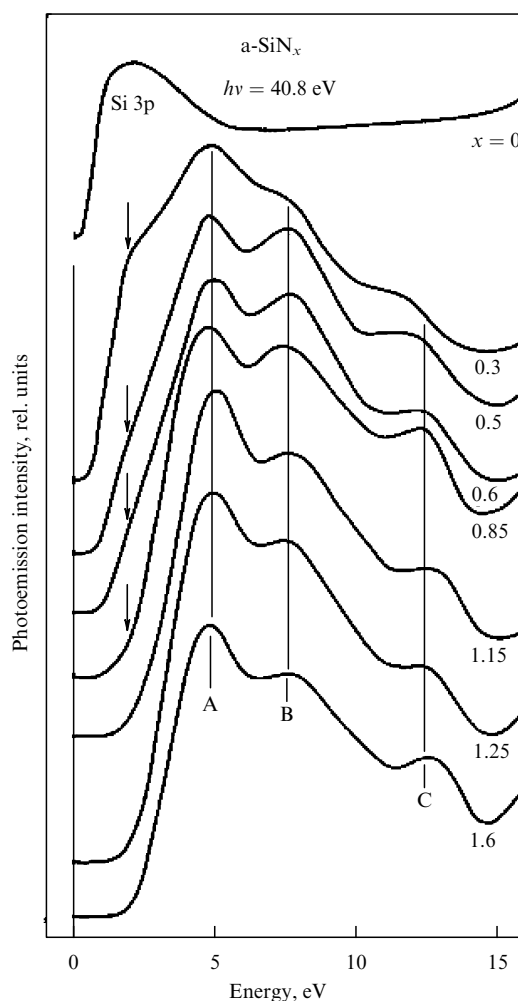

Figure 14. UV photoelectron spectra of the valence band of SiN_x.

the reason being that Si 3s, 3d states shift toward the band gap.

8. Optical properties of silicon-rich and irradiated silicon nitride

As already noted, silicon nitride is synthesized by thermally decomposing silicon- and nitrogen-containing gases (for example, SiH_4 and NH_3). Increasing the ratio SiH_4/NH_3 provides silicon nitride with an excess of silicon. Enriching SiN_x with silicon moves the fundamental absorption edge to lower energies (Fig. 17). Stoichiometric Si_3N_4 irradiated with high-energy boron ions exhibits a similar effect. Figure 18 shows the spectral dependence of the absorption coefficient of silicon nitride irradiated with various doses of boron ions [33]. Increasing the dose shifts the absorption edge to lower energies due to the shift (as shown in the preceding section) of the 2p—Si 3s, 3p, and d orbitals toward the band gap. The quantum chemical calculations illustrated in Fig. 19 (reproduced from Ref. [34]) confirm this interpretation. Enriching SiN_x with silicon decreases the gap width. It is established in [33] that irradiation does not increase the refractive index of Si_3N_4 (see Fig. 20), similarly to enriching SiN_x with silicon.
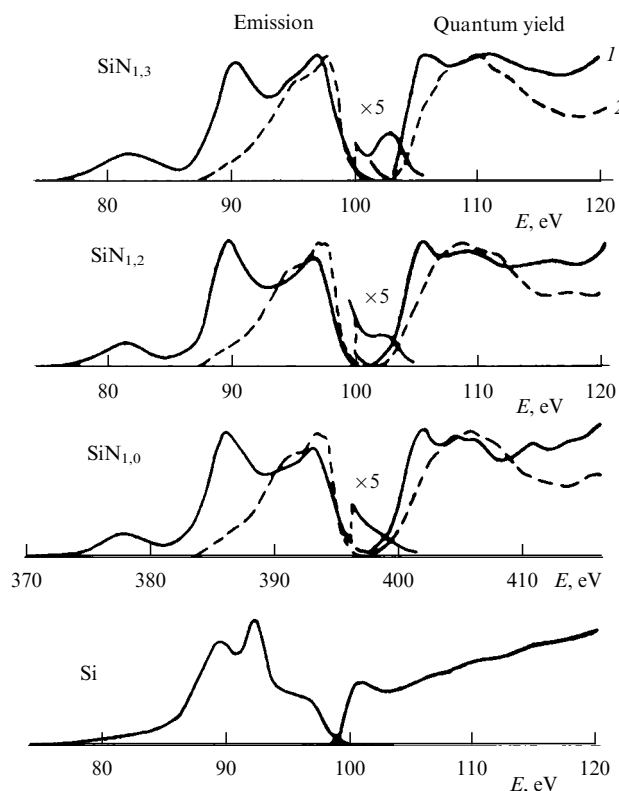
Figure 15. X-ray emission and quantum yield spectra of SiN_x of variable composition.
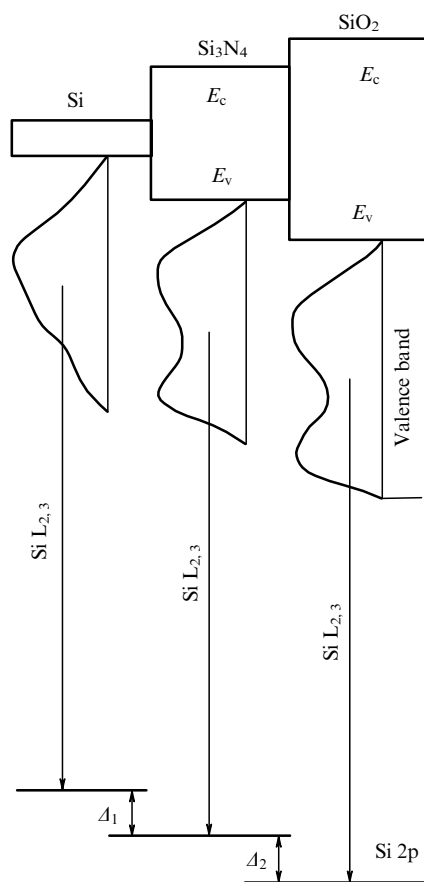

Figure 16. Shift of the Si 2p level and valence band top in tetrahedral silicon compounds Si, Si_3N_4, SiO_2.
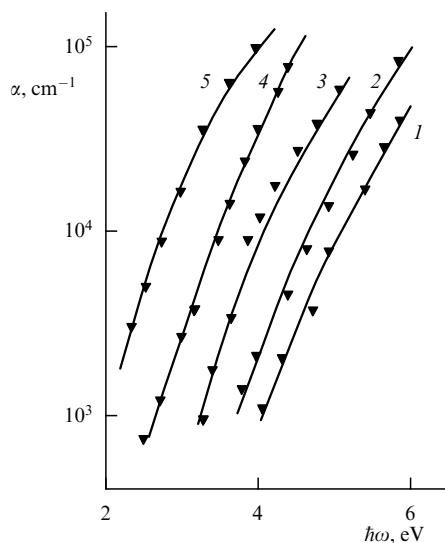

Figure 17. Spectral dependence of the absorption coefficient of SiN_x grown at various values of the ratio $R = SiH_4/NH_3$: 1:100 (*1*), 1:10 (*2*), 1:5 (*3*), 1:3 (*4*), 1:1 (*5*).
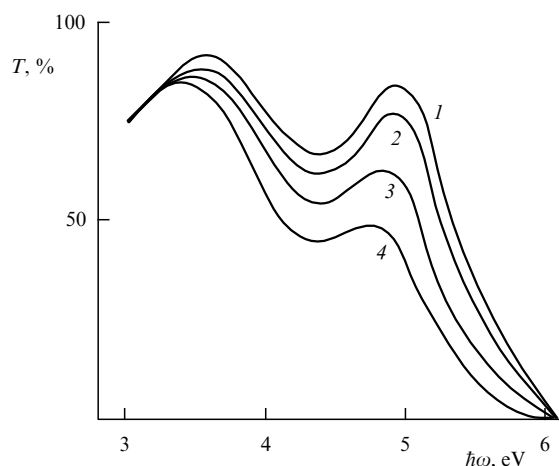

Figure 18. Spectral dependence of the absorption coefficient of silicon nitride irradiated with B^+ ions: (*1*), original Si_3N_4; (*2*)–(*4*) irradiation with B^+ ions at 100 keV at the dose $D = 3 \times 10^{12}$ (*2*), 3×10^{14} (*3*), 3×10^{15} cm^{-2}(*4*).

9. Conclusions

This paper provides a detailed examination of the electronic structure and electron and hole masses in silicon nitride. Physico-chemical calculations currently available provide a good description of the experimentally observed charge transfer in the Si–N bond.

Analysis shows that the upper valence band arises from bonding N 2p–Si $3sp^3$ orbitals. The top of the valence band is predominantly composed of nonbonding N $2p_\pi$ orbitals. It is fundamentally important to note, however, that in addition to N $2p_\pi$ orbitals, the bonding N 2p–Si $3sp^3$ orbitals also contribute to the formation of the top of the valence band. Because the overlap integral of N $2p_\pi$ orbitals is small, corresponding to such orbitals near the top of the valence band are 'heavy' holes ($m_h^* \approx 25 m_0$). Corresponding to the bonding Si $3sp^3$–N 2p near the top of the valence band are 'light' ($m_h^* \approx 0.5 m_0$) holes. Large overlap integrals correspond to these orbitals.
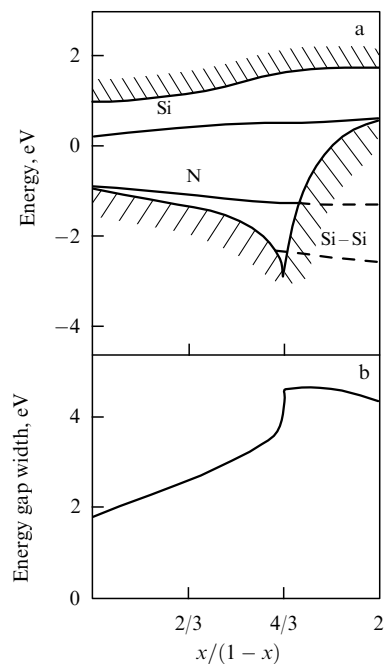
Figure 19. (a) Calculated energy diagram of SiN_x and the position of the energy gap edges and defect levels as a function of the parameter x. (b) Energy gap width of SiN_x as a function of x.
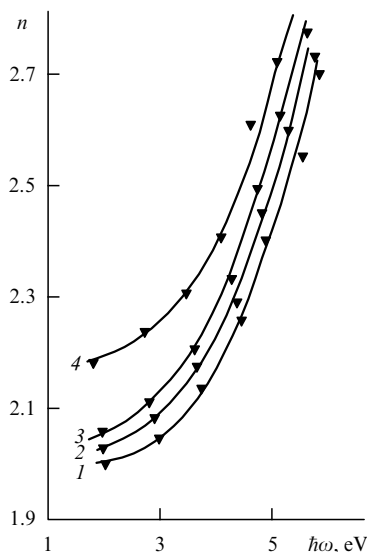

Figure 20. Spectral dependence of the refractive index of B^+-ion-irradiated silicon nitride: (*1*), original Si_3N_4; (*2*)–(*4*) irradiation with 100 keV B^+ ions at the dose $D = 3 \times 10^{12}$ (*2*), 3×10^{14} (*3*), 3×10^{15} cm^{-2} (*4*).

References

1. Gritsenko V A *Stroenie i Elektronnaya Struktura Amorfnykh Dielektrikov v Kremnievykh MDP Strukturakh* (Atomic and Electronic Structure of Amorphous Dielectrics in MDS Structures) (Novosibirsk: Nauka, 2003)
2. Gritsenko V A *Electronic Structure and Optical Properties of* Si_3N_4, *in Silicon Nitride in Electronics* (New York: Elsevier, 1986)
3. Roizin Y, Gritsenko V, in *Dielectric Films for Advanced Microelectronics* (Eds M Baklanov, M Greeen, K Maex) (Chichester: John Wiley & Sons, 2007)
4. Lee C-H, Park K-C, Kim K *Appl. Phys. Lett.* **87** 073510 (2005)
5. Nasyrov K A, Shaimeev S S, Gritsenko V A *Zh. Eksp. Teor. Fiz.* **136** 910 (2009) [*JETP* **109** 786 (2009)]
6. Gritsenko V A *Usp. Fiz. Nauk* **178** 727 (2008) [*Phys. Usp.* **51** 699 (2008)]
7. Zerr A et al. *Nature* **400** 340 (1999)
8. Mo S-D et al. *Phys. Rev. Lett.* **83** 5046 (1999)
9. Sekine T et al. *Appl. Phys. Lett.* **76** 3706 (2000)
10. Ren S-Y, Ching W Y *Phys. Rev. B* **23** 5454 (1981)
11. Xu Y-N, Ching W Y *Phys. Rev. B* **51** 17379 (1995)
12. Roberson J *Philos. Mag.* **44** 215 (1981)
13. Shaposhnikov A V, Petrov I P, Gritsenko V A, Kim S V *Fiz. Tverd. Tela* (St-Petersburg) **49** 1554 (2007) [*Phys. Solid State* **49** 1628 (2007)]
14. Perevalov T V, Gritsenko V A *Usp. Fiz. Nauk* **180** 587 (2010) [*Phys. Usp.* **53** 561 (2010)]
15. Gritsenko V A, Meerson E E, Morokov Yu N *Phys. Rev. B* **57** R2081 (1998)
16. Guo X, Ma T P *IEEE Electron Device Lett.* **19** 207 (1998)
17. Yeo Y-C, King T-J, Hu C *Appl. Phys. Lett.* **81** 2091 (2002)
18. Yu H Y et al. *IEEE Electron Device Lett.* **23** 285 (2002)
19. Yu H et al. *IEEE Trans. Electron Devices* **49** 1158 (2002)
20. Sorokin A N, Karpushin A A, Gritsenko V A, Wong H *J. Appl. Phys.* **105** 073706 (2009)
21. Nekrashevich S S, Gritsenko V A, Klauser R, Gwo S *Zh. Eksp. Teor. Fiz.* **138** 745 (2010) [*JETP* **111** 659 (2010)]
22. Gritsenko V A et al. *Fiz. Tekh. Poluprovodn.* **35** 1041 (2001) [*Semiconductors* **35** 997 (2001)]
23. Carson R D, Schnatterly S E *Phys. Rev. B* **33** 2432 (1986)
24. Yeh J-J *Atomic Calculation of Photoionization Cross-Sections and Asymmetry Parameters* (Langhorne, PA: Gordon and Breach Sc. Publ., 1993)
25. DiStefano T H, Estman D E *Phys. Rev. Lett.* **27** 1560 (1971)
26. Lieske N, Hezel R *Thin Solid Films* **61** 217 (1979)
27. Philipp H R *J. Electrochem. Soc.* **120** 295 (1973)
28. Griscom D L *J. Non-Cryst. Solids* **24** 155 (1977)
29. Gritsenko V A et al. *Phys. Rev. Lett.* **81** 1054 (1998)
30. Gritsenko V A et al. *Zh. Eksp. Teor. Fiz.* **125** 868 (2004) [*JETP* **98** 760 (2004)]
31. Bolotin V P, Brytov I A, Gritsenko V A, Popov V P *Dokl. Akad. Nauk SSSR* **310** 114 (1990)
32. Kärcher R, Ley L, Johnson R L *Phys. Rev. B* **30** 1896 (1984)
33. Gritsenko V A et al. *Dokl. Akad. Nauk SSSR* **287** 1381 (1986) [*Sov. Phys. Dokl.* **31** 341 (1986)]
34. Martin-Moreno L et al. *Phys. Rev. B* **35** 9683 (1987)